Temperature and density relaxation close to the liquid-gas critical point: An analytical solution for cylindrical cells

Pierre Carlès
Laboratoire de Modélisation en Mécanique, Université Pierre et Marie Curie, 4 place Jussieu, 75252 Paris Cedex 05, France

Fang Zhong, Mark Weilert, and M. Barmatz
Jet Propulsion Laboratory, 4800 Oak Grove Drive Pasadena, California 91109, USA
(Received 15 July 2004; revised manuscript received 10 November 2004; published 4 April 2005)

We present a study of the temperature and density equilibration near the liquid-gas critical point of a composite system consisting of a thin circular disk of near-critical fluid surrounded by a copper wall. This system is a simplified model for a proposed space experiment cell that would have 60 thin fluid layers separated by perforated copper plates to aid in equilibration. Upper and lower relaxation time limits that are based on radial and transverse diffusion through the fluid thickness are shown to be too significantly different for a reasonable estimate of the time required for the space experiment. We therefore have developed the first rigorous analytical solution of the piston effect in two dimensions for a cylindrically symmetric three-dimensional cell, including the finite conductivity of the copper wall. This solution covers the entire time evolution of the system after a boundary temperature step, from the early piston effect through the final diffusive equilibration. The calculation uses a quasistatic approximation for the copper and a Laplace-transform solution to the piston effect equation in the fluid. Laplace inversion is performed numerically. The results not only show that the equilibration is divided into three temporal regimes but also give an estimate of the amplitudes of the remaining temperature and density inhomogeneity in each regime. These results yield characteristic length scales for each of the regimes that are used to estimate the expected relaxation times in the one- and two-phase regions near the critical point.

DOI: 10.1103/PhysRevE.71.041201 PACS number(s): 44.10.+i, 05.70.Jk, 64.60.−i, 66.10.Cb

I. INTRODUCTION

In determining the feasibility of performing experiments near a liquid-gas critical point, it is important to know the expected thermal equilibration time for a given experimental arrangement. It is known that there is competition between the critical slowing down associated with the diminishing thermal diffusivity and the critical speeding up associated with the piston effect [1–5]. The piston effect is known to dominate the early stages of the thermal equilibrium process. At later times, the remaining temperature and resultant density gradients will relax diffusively. General expressions combining these two competing effects have been developed [1,2] and applied to the one-dimensional case. One-dimensional (1D) theoretical models have also been developed to describe the evolution of the temperature and density distributions in the presence of gravity and in a microgravity environment [5–8].

Berg studied the thermal equilibration in three dimensions near the critical point for the case of a thin disk of fluid [9]. His analysis provided the first insight into the effect of geometry on density and temperature equilibration. That study demonstrated the existence of isobaric modes induced by a temperature gradient that relax on a much longer time scale than that of the piston effect. Ferrell and Hao studied the composite system of a near-critical fluid and enclosing solid walls in an arbitrary geometry [10]. They showed that when temperature is measured at the outer surface of a solid wall, the fast thermal equilibration takes a longer time than when measured directly inside the fluid. This delay is due to the finite thermal conductivity of the wall. However, their study was limited to the intermediate-time regime of the piston effect, so that no practical information could be deduced as regards the relaxation of density (which takes place on the diffusion time scale). Up to now, there has been no model that includes the effects of both geometry and finite conductivity of the container solid walls for a complete temporal coverage from the initial fast adiabatic equilibration to the final diffusive relaxation. The development of such a model is the aim of the present work.

We will present in this paper a study of temperature and density equilibration of a composite system consisting of a thin circular disk of near-critical fluid surrounded by a copper wall. Such geometry has been used in several Earth-bound experiments and proposed space-based experiments on near-critical fluids [11,12]. A small cell gap is chosen to reduce the density stratification on the Earth and the long relaxation times both on the Earth and in space. A large cell diameter provides a large sample size for increased signal-to-noise ratio in specific heat measurements. In this paper, we will determine the thermodynamic behavior of such a system from the early piston effect regime all the way to final equilibrium. The results of our calculation will be used to estimate equilibration times for a much more complicated experimental cell being considered for a future space experiment. Because the fluid relaxation time is the longest along the critical isochore, all our numerical estimations were made for the case of the critical isochore. The thermodynamic properties of ^{3}He were calculated using the information collected in Ref. [6].

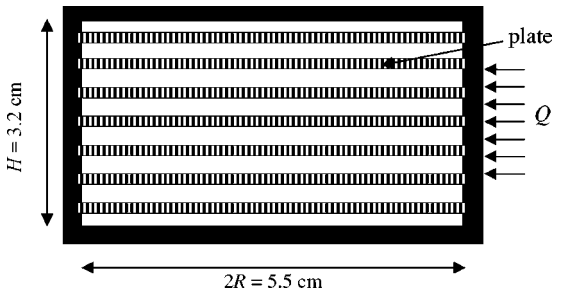

FIG. 1. Sketch of the flight experimental cell. Heat is applied at cell boundaries. Plates are not shown to scale.

II. BACKGROUND

The motivation for performing this study was to design an experimental cell for efficiently measuring the specific heat near the critical point of ^{3}He in a microgravity environment. Because a large gravity-induced density stratification is no longer a problem in a microgravity environment, one would like to increase the sample size in order to increase the signal-to-noise ratio for a specific heat measurement. At the same time, a slow diffusive relaxation associated with the large sample size should be avoided due to limited flight time in space. In order to reconcile these two conflicting requirements, a composite cylindrical cell design has been proposed for a future space flight [12]. Figure 1 shows a schematic of the cell design being considered. The cell has a 5.5 cm inner diameter and a 3.2 cm height and contains a stack of copper plates with copper spacers. Each plate and spacer is 0.025 cm thick. With this arrangement, the bulk fluid is separated into 64 equally thin layers. There are many holes in the copper plates, so the fluid in each layer can communicate with the fluid in adjacent layers. The copper plates are thermally linked to the temperature-regulated copper walls (i.e., the circumference boundary) and act as thermal shorts to speed up the equilibration in the bulk fluid.

In estimating the time required for a future space experiment, it is important to determine the expected equilibration time constant for such a cell design. Because specific heat is a strong function of density near the critical point, its measurement should be taken after both temperature and density inhomogeneity relax to within prescribed values respectively. For a fluid in the single phase, such as the critical isochore above the critical temperature T_c, the relaxation time for specific heat measurements using a pulse heat is not a major concern since the piston effect speeds up the temperature equilibration. The large density inhomogeneity at boundaries, induced by the piston effect, causes less than 1% systematic error in the total heat capacity very close to T_c since the boundary layers are so narrow. However, in coexisting phases below T_c, diffusive density relaxation will affect the temperature relaxation directly due to the latent heat caused by the mass conversion. Since there are two characteristic length scales for this cell design, two different diffusive relaxation times are expected. We would like to determine how to utilize these two length scales to estimate the time required for specific heat measurements in the coexisting phases.

We started by using a 1D approximation to find the upper and lower bounds for thermal relaxation of one fluid layer in the single phase and eventually found an approximation to estimate the relaxation time in coexisting phases. If the copper plates are perfect conductors, the temperature of the plates will instantly follow that of the external copper wall. Any radial inhomogeneity in the fluid layer will be removed immediately via the copper plates. The fluid will then equilibrate by transverse conduction through the thickness of the layer. The thermal relaxation time (different from the usual Fourier expression at constant pressure) is [1]

$$\tau_{\text{transverse}} = \frac{(\rho C_P)_{\text{He}}}{\lambda_{\text{He}}}\left(\frac{d_{\text{He}}}{2\pi}\right)^2, \tag{1}$$

where C_P and λ are the specific heat at constant pressure and thermal conductivity respectively, ρ is the fluid density, and d_{He} is the thickness of the fluid layer. Equation (1) implies that the characteristic length scale is the fluid layer thickness between the copper plates.

On the contrary, if the copper plates are poor conductors, an inhomogeneity will be relaxed radially through the fluid to the sidewalls,

$$\tau_{\text{radial}} = \frac{1}{Dk^2} = \frac{1}{2}\frac{(\rho C_P)_{\text{He}}}{\lambda_{\text{He}}}\left(\frac{2R_{\text{He}}}{\pi}\right)^2. \tag{2}$$

Equation (2) implies that the characteristic length scale is the radius R of the fluid layer. Because of the huge difference in the length scales, the relaxation times of the two cases are very different, $\tau_{\text{radial}} = 2(2R/d)^2\tau_{\text{transverse}} = 9.68\times 10^4\tau_{\text{transverse}}$. The expression for τ_{radial} gives an unrealistically large upper limit on the relaxation time because it totally ignores the contribution of conduction in the copper plates. We therefore next considered a composite system of a fluid layer and a copper plate in contact. The specific heat $(\rho C_P)_{\text{He}}$ of helium is much larger than that of the copper $(\rho C_P)_{\text{Cu}}$, the ratio $(\rho C_P)_{\text{He}}/(\rho C_P)_{\text{Cu}}$ being ~ 350 at $T/T_c - 1 = 10^{-2}$ and increasing for smaller reduced temperatures. The thermal conductivity of copper, λ_{Cu}, is much larger than that of the helium, λ_{He}, the ratio $\lambda_{\text{Cu}}/\lambda_{\text{He}}$ being $\sim 10^4$ at $T/T_c - 1 = 10^{-6}$ and increases for larger reduced temperatures. We can intuitively approximate the average properties of the composite system and substitute them into the expression for τ_{radial}:

$$\tau_{\text{radial}}^{\text{comp}} = \frac{1}{2}\frac{d_{\text{He}}}{d_{\text{He}} + d_{\text{Cu}}}\frac{(\rho C_P)_{\text{He}}}{\dfrac{d_{\text{Cu}}}{d_{\text{He}} + d_{\text{Cu}}}\lambda_{\text{Cu}}}\left(\frac{2R}{\pi}\right)^2$$

$$= \frac{1}{2}\frac{d_{\text{He}}}{d_{\text{Cu}}}\frac{(\rho C_P)_{\text{He}}}{\lambda_{\text{Cu}}}\left(\frac{2R}{\pi}\right)^2, \tag{3}$$

where d_{Cu} is the thickness of the copper plate. A realistic relaxation time for a given reduced temperature $T/T_c - 1$ will be bounded by the two extremes, τ_{trans} and $\tau_{\text{radial}}^{\text{comp}}$ as shown in Fig. 2. Whether the realistic relaxation time follows the upper bound or the lower bound depends on whether the copper plate can be considered isothermal. In Appendix A, we use a simple model to show that the radial temperature difference in the copper plate ΔT_{Cu} is less than 1% of the temperature step change ΔT at the side wall for $T/T_c - 1 < 10^{-4}$ using a

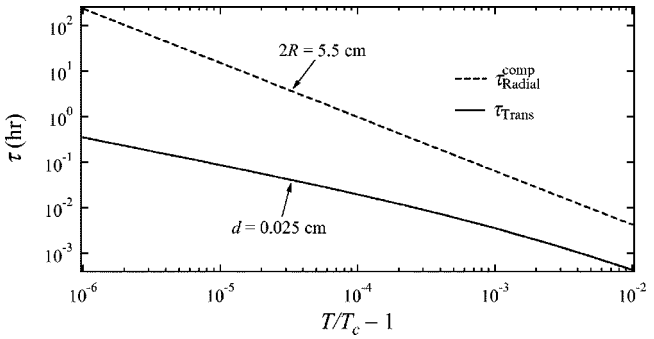

FIG. 2. Transverse and composite radial relaxation times versus reduced temperature for ^{3}He fluid along its critical isochore.

modified piston time. Because this simple model predicts nearly isothermal copper, it suggests that the true relaxation time is close to the faster ($\tau_{transverse}$) limit shown in Fig. 2.

A. Rigorous calculation of piston effect for a cylindrical composite 3D cell

The range of relaxation times presented in Fig. 2 is so large that we need a better estimate of the characteristic length scale for the equilibration of the stacked cell. A piston effect model for a cylindrically symmetric three dimensional (3D) cell was developed to address this problem. In this model, the complete entropy transfer equation, as first proposed by Onuki *et al.* [2], is used to model thermal relaxation in the fluid and the conventional heat transfer equation is used in the copper plate. The explicit solution obtained in Laplace space contains the early piston effect regime and the late diffusive relaxation regimes as well as the transition between the different regimes. This solution does not require the use of the asymptotic matching techniques between time scales of these regimes.

In order to simplify the problem, we analyzed the thermal behavior of a composite system consisting of a single fluid layer plus a copper plate located in the middle of the stacked cell shown in Fig. 3. This part of the cell is far enough from the top and bottom cell boundaries that thermal relaxation in this region can be considered equivalent to that observed in an infinite periodic stack of such pairs. Actually there are 64 stacked pairs in the flight cell design and our analysis on the middle pair can serve as the worst-case estimate for the equilibration time of all other pairs. Due to symmetry and periodicity, only the area enclosed by the thick rectangle needs to be considered. The thickness of the copper layer is an adjustable parameter in our model, so the most general solution will be obtained. The boundary conditions shown in Fig. 3 are as follows: the circumference boundary of the two cylindrical layers is subjected to a step temperature change, ΔT, while the top and bottom boundaries are considered to be adiabatic.

The governing equation in the copper is the conduction equation written for cylindrical geometry with axial symmetry (the variables being r and z):

$$\frac{\partial T}{\partial t} - D_{\mathrm{Cu}}\left\{\frac{1}{r}\left[\frac{\partial}{\partial r}\left(r\frac{\partial T}{\partial r}\right)\right] + \frac{\partial^2 T}{\partial z^2}\right\} = 0. \tag{4}$$

The governing equation in the helium is the piston-effect equation [2]

$$\frac{\partial T}{\partial t} = \frac{\gamma - 1}{\gamma}\frac{\partial \langle T\rangle}{\partial t} + D_{\mathrm{He}}\left\{\frac{1}{r}\left[\frac{\partial}{\partial r}\left(r\frac{\partial T}{\partial r}\right)\right] + \frac{\partial^2 T}{\partial z^2}\right\}, \tag{5}$$

where $\langle T\rangle$ represents the spatial average of T and $\gamma \equiv C_P/C_V$ is the ratio of the heat capacities. $\langle T\rangle$ is a function of time only. It should be noted that these equations are valid only in the linear regime where the changes of the media properties are negligible over the induced temperature change.

B. Calculation in copper

Equation (4) can be made nondimensional using the change of variables

$$t^* = \frac{t}{t_D^{\mathrm{He}}}, \quad r^* = \frac{r}{R}, \quad \overline{z} = \frac{z}{d_{\mathrm{Cu}}/2}. \tag{6}$$

Here $t_D^{\mathrm{He}} = (d_{\mathrm{He}}/2)^2/D_{\mathrm{He}}$ is the transverse heat diffusion time in the fluid helium and similarly $t_D^{\mathrm{Cu}} = R^2/D_{\mathrm{Cu}}$ is the radial heat diffusion time of the copper plate. Using $H = d_{\mathrm{Cu}}/(2R)$ and ignoring the superscript stars for t and r from now on, the nondimensional equation for copper becomes

$$\frac{t_D^{\mathrm{Cu}}}{t_D^{\mathrm{He}}}\frac{\partial T}{\partial t} - H^2\frac{1}{r}\left[\frac{\partial}{\partial r}\left(r\frac{\partial T}{\partial r}\right)\right] - \frac{\partial^2 T}{\partial \overline{z}^2} = 0. \tag{7}$$

Since $t_D^{\mathrm{Cu}}/t_D^{\mathrm{He}} < 10^{-5}$ for all reduced temperatures, the temperature in copper, $\overline{T}(r,\overline{z},t)$, is governed to first-order by the equation

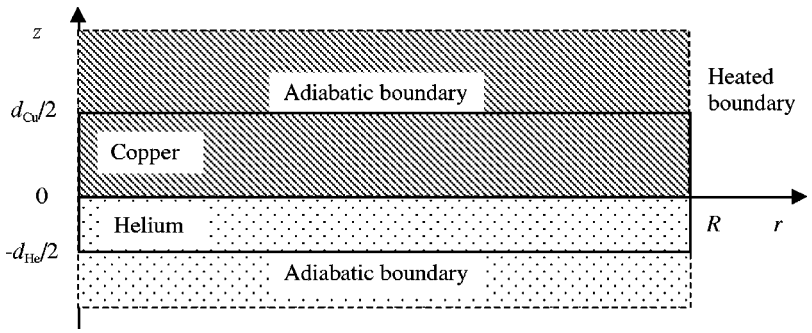

FIG. 3. Illustration of a 2D composite system and its boundary conditions.

$$H^2 \frac{1}{r}\left[\frac{\partial}{\partial r}\left(r\frac{\partial \overline{T}}{\partial r}\right)\right] + \frac{\partial^2 \overline{T}}{\partial \overline{z}^2} = 0, \tag{8}$$

with

$$\frac{T - T_i}{\Delta T} = \overline{T}(r,\overline{z},t) + O\left(\frac{t_D^{\mathrm{Cu}}}{t_D^{\mathrm{He}}}\right), \tag{9}$$

where T_i is an initial temperature.

This result shows that the temperature in the copper layer is quasistatic to first order. The copper temperature follows a Poisson equation with fixed boundary conditions, in which time is a parameter but not a variable. It is solved by variable separation. Inserting $\overline{T}(r,\overline{z}) \equiv f(r)g(\overline{z})$ into Eq. (8) leads to

$$\frac{1}{f}\frac{1}{r}(rf')' = -\frac{1}{H^2}\frac{g''}{g} = -C^2, \tag{10}$$

where C is a real constant. The solutions of these two equations are

$$g(\overline{z}) = a(t)\cosh[CH(z-1)], \tag{11}$$

$$f(r) = J_0(Cr), \tag{12}$$

with a being a real function of t and $J_0(r)$ being the Bessel function of zero order. Equation (11) satisfies the adiabatic boundary condition at the top of the copper plate ($\overline{z}=1$). The following form is then chosen for $\overline{T}$ for the case of an imposed temperature at the outer border of the copper and helium layers—i.e., $\overline{T}(r=1,\overline{z},t)=1$:

$$\overline{T}(r,\overline{z},t) = 1 - \sum_{1}^{+\infty} a_n(t)\cosh[C_n H(\overline{z}-1)]J_0(C_n r), \tag{13}$$

with the C_n's being the roots of J_0. Note that this specific form (and the subsequent solutions) could be generalized to more complex temperature boundary conditions in a straightforward manner.

C. Calculation in helium

The vertical dimension in helium is scaled by $d_{\mathrm{He}}/2$ as

$$\tilde{z} = \frac{z}{d_{\mathrm{He}}/2}. \tag{14}$$

Equation (5) is now made nondimensional. We now have

$$\frac{\partial T}{\partial t} = \frac{\gamma - 1}{\gamma}\frac{\partial \langle T\rangle}{\partial t} + \left(\frac{d_{\mathrm{He}}/2}{R}\right)^2 \frac{1}{r}\left[\frac{\partial}{\partial r}\left(r\frac{\partial T}{\partial r}\right)\right] + \frac{\partial^2 T}{\partial \tilde{z}^2}. \tag{15}$$

Since $d_{\mathrm{He}}/2 \ll R$, the temperature perturbation in the helium, $\tilde{T}(r,\tilde{z},t)$, is governed to first order by the equation

$$\frac{\partial \tilde{T}}{\partial t} = \frac{\gamma - 1}{\gamma}\frac{\partial \langle \tilde{T}\rangle}{\partial t} + \frac{\partial^2 \tilde{T}}{\partial \tilde{z}^2}, \tag{16}$$

with

$$\frac{T - T_i}{\Delta T} = \tilde{T}(r,\tilde{z},t) + O\left(\frac{d_{\mathrm{He}}/2}{R}\right). \tag{17}$$

In other words, the radial heat diffusion in helium (along r) is considered negligible compared to the transverse diffusion (along z). One consequence of this approximation is that the local radial heat into the fluid at the circumference copper wall will not be taken into account in the final solution. The only heat into the fluid will be through the copper plates after the copper plates are very rapidly heated to almost the same temperature as the circumference wall over their own typical relaxation times. Although this may sound like a severe assumption, it is in fact totally relevant to the chosen geometry since the wetted surface of the copper plates is 45 times larger than the wetted surface of the circumference wall, even though the fluid is heated simultaneously by the circumference copper wall and by the copper plates.

Equation (16) is solved by means of Laplace transforms. Letting p be the Laplace parameter associated with the nondimensional time variable t, Eq. (16) now becomes

$$p\tilde{T} - \frac{\partial^2 \tilde{T}}{\partial \tilde{z}^2} = \frac{\gamma - 1}{\gamma} p\langle \tilde{T}\rangle, \tag{18}$$

with a solution in the form

$$\tilde{T} = \frac{\gamma - 1}{\gamma}\langle \tilde{T}\rangle(p) + b(p,r)\cosh[\sqrt{p}(z+1)]. \tag{19}$$

Equation (19) satisfies the adiabatic boundary condition at the bottom of the helium layer ($\tilde{z}=-1$).

By matching the heat flux and temperature at the interface between helium and copper, we derive an analytical expression for spatial temperature distribution in Laplace space. One needs only to invert the Laplace transforms to obtain the temperature profiles and average temperature at any given time. The details of the derivation and the expression are given in Appendix B. The obtained solution is verified by the test cases described in Appendix C. The procedure for the Laplace inversion, conducted numerically, is described in Appendix D.

D. Calculation of the pressure and density distributions

The pressure and density distributions are obtained by considering a linearized equation of state in the form

$$\rho - \rho_i = \left(\frac{\partial \rho}{\partial P}\right)_T (P - P_i) + \left(\frac{\partial \rho}{\partial T}\right)_\rho (T - T_i). \tag{20}$$

The pressure distribution throughout the evolution is assumed to be homogeneous since the pressure gradient relaxes on an acoustic time scale that is much shorter than the time scales of the piston effect and the later diffusion process. Recent results on bulk viscosity [13,14] have shown, however, that the assumption of a homogeneous pressure may fail very close to the critical point, where viscous stresses can build up in the thermal boundary layers and create a local pressure gradient. According to theoretical predictions [14], one consequence of this viscous effect is that the piston effect should undergo a phase of critical slowing down very close to the critical point, where its typical time scale becomes dominated by bulk viscosity. In principle, the present model should be valid only in the nonviscous region

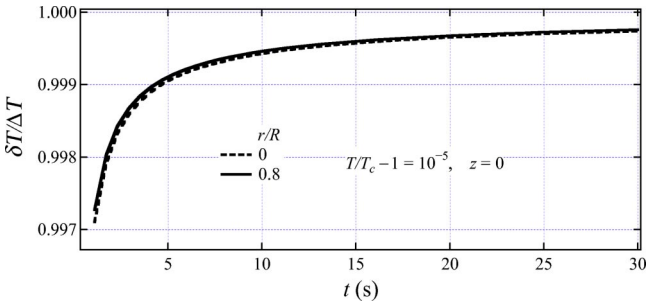

FIG. 4. The temperature evolution at a reduced temperature 10^{-5} and at the fluid copper interface for two different radial positions.

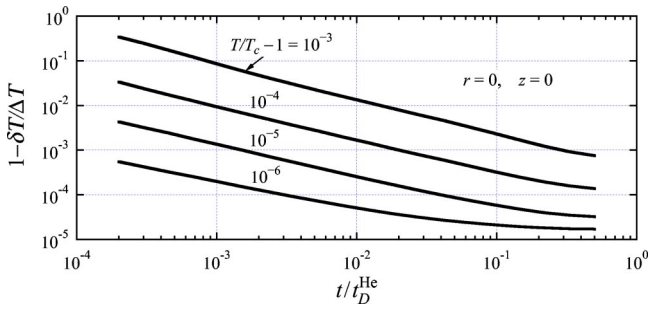

FIG. 5. The evolution of the temperature difference between the cell center and circumference boundary at the copper-fluid interface for several reduced temperatures.

of reduced temperatures above 10^{-3} when one applies formulas in [14] using $d_{He}/2 = 0.0125$ cm as a typical length scale. However, the effect of bulk viscosity can only be felt on the early piston-effect regime, and it has no consequence either on the late piston-effect relaxation or on diffusive processes and, in particular, no consequence on the diffusion-dominated density relaxation. Neglecting the bulk viscosity in the present solution should only lead to a slight underestimation of the typical time scale of temperature relaxation by the piston effect very close to the critical point. Because the average density deviation in the closed cell is zero, the spatial integration of Eq. (20) leads to

$$P - P_i = \left(\frac{\partial P}{\partial T}\right)_\rho \Delta T \langle \tilde{T} \rangle. \tag{21}$$

The density distribution is then given by

$$\rho - \rho_i = \left(\frac{\partial \rho}{\partial T}\right)_P \Delta T (\tilde{T} - \langle \tilde{T} \rangle). \tag{22}$$

III. RESULTS

The evolution of the temperature and density has been computed for several reduced temperatures and at different locations in the fluid cell, using the length scales $d_{He} = d_{Cu} = 0.025$ cm and $2R = 5.5$ cm. Shown in Fig. 4 is the temperature evolution at the fluid-copper interface for a reduced temperature 10^{-5} and for two different radial positions, $r = 0$ at the center of the cell and $r = 0.8R$ close to the circumference boundary where the step ΔT is applied. The temperature increases rapidly in the copper plate. Only 0.1% temperature inhomogeneity remains after 5 s due to the piston effect. This remaining inhomogeneity will vanish diffusively.

Figure 5 shows the residual temperature difference between the cell center and circumference boundary at the copper-fluid interface for several reduced temperatures (between 10^{-3} and 10^{-6}). A careful look at the vertical scales shows that the radial temperature gradient in the copper plate goes to zero as the critical point is approached. At a reduced temperature 10^{-3}, this temperature difference remains small (less than 10% of ΔT for $t > 10^{-3} t_D^{He}$), confirming the simplified model prediction that the copper plate is almost isothermal.

Figure 6 shows the evolution of the temperature change at several radial positions in the midplane of the helium fluid for a reduced temperature 10^{-3}. It clearly shows two distinct regimes: one is the piston-effect-dominated regime where the temperature in the bulk helium is the same regardless of the radial position; the other is the diffusion-dominated regime where the temperature relaxation in helium is influenced by the remaining temperature gradient in copper.

Although these first two regimes are observable through the temperature evolution, a third regime is only observable via the density evolution because of the diverging thermal expansion coefficient that "exposes" the remaining temperature inhomogeneity in the fluid [see Eq. (22)].

A. Three regimes in the equilibration process

1. $t/t_D^{He} \ll 1$: piston-effect regime

The early stage behavior of the system occurs for $t/t_D^{He} \ll 1$. In this piston-effect regime, heat diffuses through the copper plate into the helium layer. A thin boundary layer is created in the helium close to the copper wall. The boundary layer expansion drives a global piston effect in the whole fluid, and the bulk helium temperature increases homogeneously. Figure 7(a) illustrates the heat-flow pattern during the early piston time period when heat transfer is governed by conduction in copper and piston effect in helium. Figure 7(b) shows a calculated spatial density profile scaled by the temperature change at the circumference boundary. The calculation was made for a reduced temperature of 1×10^{-5} and $t/t_D^{He} = 0.01$ ($t = 37$ s). Both the temperature and density are dimensionless. Close to the copper-fluid interface, the fluid

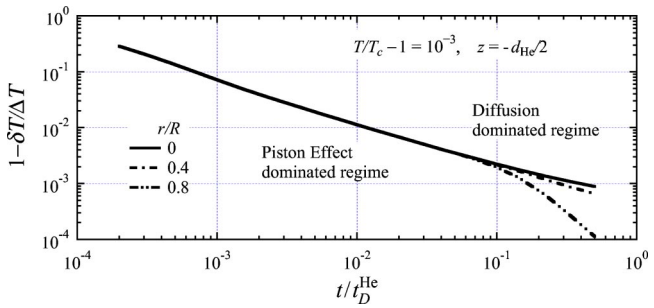

FIG. 6. The evolution of temperature change at several radial positions in the midplane of the helium fluid for a reduced temperature 10^{-3}.

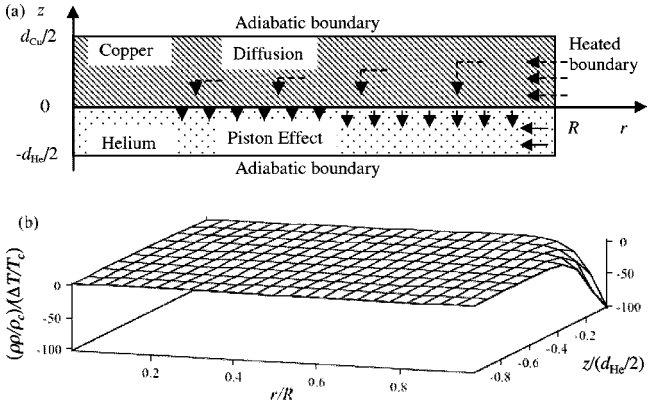

FIG. 7. (a) Heat-flow pattern during the early piston time period. (b) Calculated spatial density profile for reduced temperature 1×10^{-5} and $t/t_D^{He}=0.01$ ($t=37$ s). The dimensionless density change was scaled by the dimensionless temperature change at the circumference boundary.

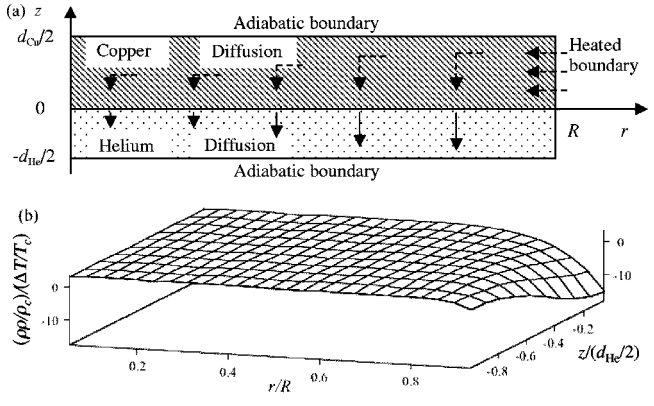

FIG. 8. (a) Heat-flow pattern during the transverse diffusion period. (b) Calculated spatial density profile for reduced temperature 1×10^{-5} and $t/t_D^{He}=0.1$ ($t=370$ s). The dimensionless density change was scaled by the dimensionless temperature change at the circumference boundary.

density undergoes a strong drop due to the thermal expansion of the boundary layer. This drop is more pronounced near the circumference border, where the copper plate is hotter. We note here that no boundary layer is observed at the circumference wall (i.e., at $r/R=1$) due to the disappearance of the radial diffusion term in the piston-effect equation (16) in helium. Had this term been kept in the asymptotic process, a strong and localized density drop would also have been observed at $r/R=1$ for all values of z. The discussion following Eq. (16) justifies that this local simplification has no consequence on the prediction of the global relaxation process. A small homogeneous density increase of the bulk fluid everywhere away from the boundary layers also occurs.

2. $0.1<t/t_D^{He}<1$: *transverse diffusion regime*

On the typical time scale of pure diffusion across the helium layer, the piston effect slowly vanishes. The boundary layer starts to diffuse deep into the helium layer, and the density and temperature gradients along the direction z are progressively relaxed by transverse heat diffusion. Figure 8(a) illustrates the heat-flow pattern during the transverse diffusion period when heat transfer is governed by conduction in copper and transverse diffusion in helium. Figure 8(b) shows a similar plot as Fig. 7(b) but at $t/t_D^{He}=0.1$ ($t=370$ s). One can observe density gradients extending along the whole fluid layer's thickness (as opposed to the localized gradients observed in the first regime). These gradients, again, are strongest near the circumference, where the temperature of the copper boundary is higher.

3. $t/t_D^{He}>1$: *Radial diffusion regime*

After this second regime, the boundary layer has totally diffused across the helium layer, and all transverse gradients have relaxed. Only radial temperature and density gradients remain in the cell, and these gradients relax radially through conduction in the copper. This can be identified as a third regime, called the radial diffusion regime. At this point, the temperature gradients are so small that the system seems to have completely relaxed to equilibrium if one examines the temperature evolution alone. On the other hand, even though over 99% temperature equilibration is completed in the first two regimes in a short time, the residual temperature inhomogeneity will still cause a substantial density inhomogeneity due to the diverging thermal expansion coefficient. Any accurate density measurement will have to wait until this density inhomogeneity relaxes. In the coexisting phases at $T<T_c$, the density relaxation will affect the temperature relaxation directly due to the latent heat caused by the mass conversion. Therefore a detailed study of the third regime in this composite geometry is necessary and the only verification of this third regime is through density relaxation measurements. Figure 9(a) illustrates the heat-flow pattern during the radial diffusion regime: heat transfer is governed by radial diffusion in the composite copper-helium system. Figure 9(b) shows a snapshot of the spatial density profile similar to Fig. 8(b) but at $t/t_D^{He}=3$ ($t=3$ h). By this time, only the radial density inhomogeneity is observable: all transverse gradients (along z) have relaxed long before (in the second regime).

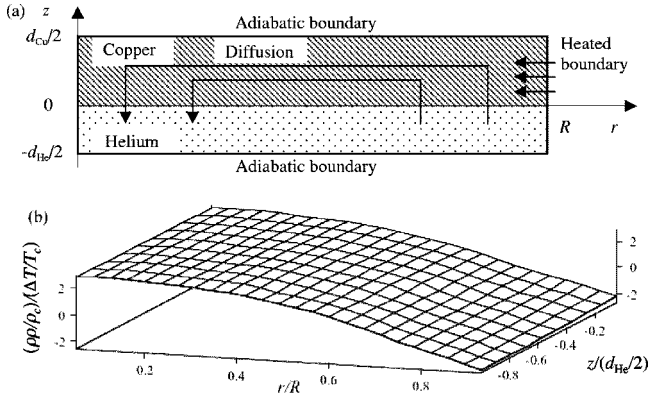

FIG. 9. (a) Heat-flow pattern during the radial diffusion period. (b) Calculated spatial density profile for reduced temperature 1×10^{-5} and $t/t_D^{He}=3$ ($t=3$ h). The dimensionless density change was scaled by the dimensionless temperature change at the circumference boundary. The vertical scale here is much more sensitive than the corresponding ones in Figs. 7 and 8.

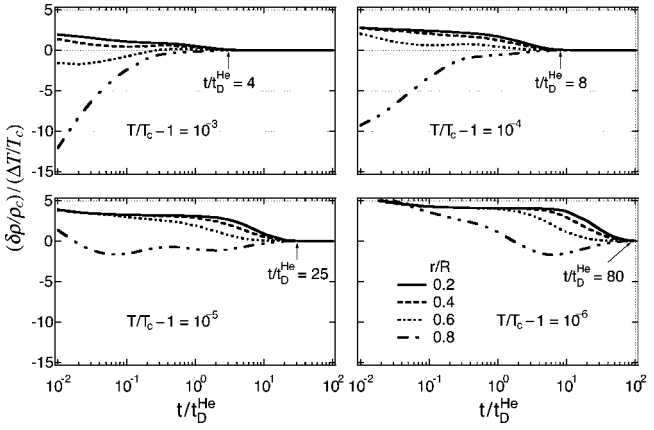

FIG. 10. Density evolution $\delta\rho=\rho-\rho_c$ at the copper-fluid interface for different reduced temperatures. The time at which the density becomes homogeneous is marked.

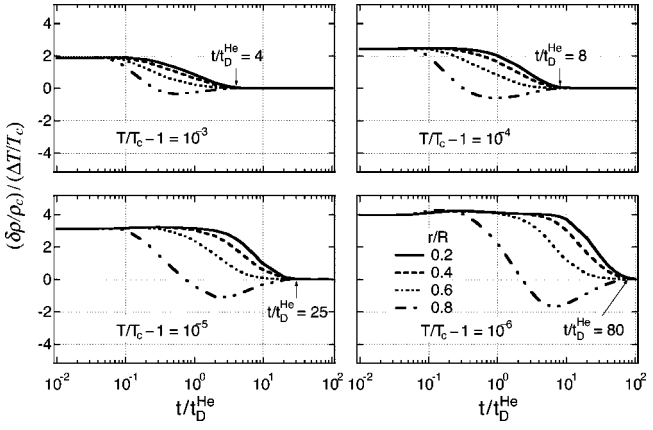

FIG. 11. Density evolution $\delta\rho=\rho-\rho_c$ in the middle of helium layer for different reduced temperatures. The time at which the density becomes homogeneous is marked.

The density evolution at different cell locations will now be discussed. Figure 10 shows the density evolution at the interface between the copper plate and ^{3}He fluid layer for four different reduced temperatures. At small radial positions, the density increases even next to the copper wall. This observation may seem surprising at first since the density could be expected to decrease close to the heated copper wall where the fluid is heated by conduction. This unexpected phenomenon, in fact, is a result of the cylindrical geometry and a purely 3D effect. When the piston effect is driven in the fluid cell by the boundary heating, the strongest boundary layer expansion occurs where the copper wall is hotter—that is, close to the circumference boundary. This strong expansion of the most external parts of the fluid layer (for large r) drives a global compression of the bulk fluid, thus increasing its density. Hence, there are two competing effects at the same time close to the center of the cell and at the copper interface. One is the local conductive heating of helium from the copper that drives a thermal expansion of the fluid (thus reducing density) and another is the global compression of the bulk fluid by the piston effect that increases the overall density of the most internal part of the fluid (for small r). The positive density variation observed at the fluid-copper interface for small values of r shows that the piston effect global compression overcomes the local thermal expansion of the fluid, at least in the first steps of the relaxation.

Figure 11 shows the density evolution in the middle of the helium layer where the density increases initially due to the piston effect. This increase is first homogeneous and then the differences at different radial positions become substantial when transverse diffusion starts pervading the cell (i.e., for times of $t/t_D^{\mathrm{He}}\sim 1$). This is the indication of entering the so-called transverse diffusion regime, dominated no longer by the piston effect but by transverse diffusion.

Both close to the copper walls and in the middle of the helium layer, the typical time t_{RD} for the scaled remaining radial density inhomogeneity $(\delta\rho/\rho_c)/(\Delta T/T_c)=0.1$ is longer than the pure transverse diffusion time across the helium layer t_D^{He} (as shown by arrows in Figs. 10 and 11). This radial relaxation time becomes longer as the critical point is approached. Its value is typically $\tau_{RD}/t_D^{\mathrm{He}}\sim 5$, 10, 40, and 100 for reduced temperatures of 10^{-3}, 10^{-4}, 10^{-5}, and 10^{-6}, respectively. This is still much faster than pure diffusion in helium along the radius, which takes a time $t/t_D^{\mathrm{He}}\sim 5000$. Figure 12 shows the equilibration time (thick solid line) for the radial density inhomogeneity, τ_{RD}, versus reduced temperature. Also shown in Fig. 12 are τ_{trans} (thin solid line) and $\tau_{\mathrm{radial}}^{\mathrm{comp}}$ (dashed line) for $T>T_c$ previously shown in Fig. 2. It is very interesting to note that τ_{RD} is parallel to $\tau_{\mathrm{radial}}^{\mathrm{comp}}$ in the logarithmic plot, indicating that the two are linked to the same length scale and have the same reduced temperature dependence. Considering that τ_{RD} corresponds to the radial density inhomogeneity equals to $(\Delta T/T_c)10\%$ while $\tau_{\mathrm{radial}}^{\mathrm{comp}}$ is the relaxation time for an exponential decay, it is not surprise that τ_{RD} is longer than $\tau_{\mathrm{radial}}^{\mathrm{comp}}$ by approximately a factor of 2. We thus associate $\tau_{\mathrm{radial}}^{\mathrm{comp}}$ with the relaxation time for radial density inhomogeneity. This is an important discovery of our 3D piston-effect solution for a composite system with the boundary conditions defined in Fig. 3.

The relaxation in the third regime can also be associated with the isobaric modes discussed by Berg [9] and Wilkinson *et al.* [15]. These modes are characterized by an asymmetric temperature distribution with one part of the fluid cooling by transferring heat to the wall and another part warming by

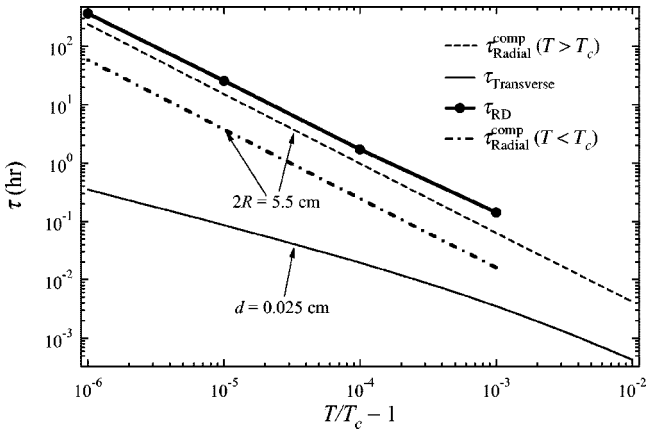

FIG. 12. Various characteristic times versus reduced temperature.

extracting heat from the wall, just as shown in Fig. 9. In the current results, the long relaxation time for the third regime is caused by the finite conductivity of the copper. This was not seen in [9] which assumed perfectly isothermal boundary conditions, but it was hinted at by a significant conductivity correction calculated even for an infinitely thick, high-conductivity sapphire cell wall in Ref. [15].

The result obtained in this analysis can easily be extended to the two-phase case. Indeed, Zhong and Meyer proved in their early work [16] that the density relaxation in coexisting phases for $T<T_c$ could be approximated with the average thermal properties of the two phases. Since a density relaxation is directly linked to a temperature relaxation in coexisting phases as $\delta\rho_{\mathrm{liq}} \propto -\beta(1-T/T_c)^{\beta-1}(\delta T/T_c)$ where $\beta=0.325$ is the critical exponent for the coexistence curve, this radial relaxation time can also be used to estimate the temperature relaxation time in the coexisting phases. Substituting the average specific heat at constant pressure into Eq. (3) for the composite relaxation time, we obtain the temperature relaxation time for the same composite system in the coexisting phases as shown by the dot-dashed line in Fig. 12. The estimated radial relaxation time in the coexisting phases is about 4 times shorter than in the single phase. This factor of 4 comes from the fact that the specific heat at constant pressure is proportional to the isothermal susceptibility. Based on the restricted cubic model equation of state, the isothermal susceptibility is about a factor of 4 smaller in the coexisting phases than in the single phase along the critical isochore.

B. Equilibration in specific heat measurements

For the specific heat measurement along the critical isochore above the critical temperature T_c, a temperature equilibration is completed to within 1% in seconds due to the piston effect. Thus, we can use the lower bound τ_{trans} in Fig. 12 to safely estimate the time required for such a measurement in the single phase. This relatively short time will permit measurements to be performed over a reduced temperature range $10^{-6} \leqslant T/T_c-1 \leqslant 10^{-3}$. However, in coexisting phases below T_c, the temperature relaxation time $\tau_{\mathrm{radial}}^{\mathrm{comp}}$ is about 60 h at $|T/T_c-1| \sim 10^{-6}$ as shown in Fig. 12. Considering that there is about a factor of 2 between the composite relaxation time $\tau_{\mathrm{radial}}^{\mathrm{comp}}$ (dashed line) and 1% cutoff density equilibration time τ_{RD} (thick solid line), it will take approximately 120 h to obtain heat capacity measurements with a precision of 1% at $\sim 10^{-6}$. To permit a better level of 0.1% precision in C_V measurements during a limited space flight time, one can limit measurements to only $|T/T_c-1| \geqslant 10^{-5}$ where the temperature equilibration time for a 0.1% precision would be ~ 8 h. The equilibration time would be shorter if less stringent demands are made on the precision of a C_V measurement.

Haupt and Straub measured the specific heat of SF_6 in microgravity using a spherical cell of 19.2 mm diameter [17]. They used a continuous calorimetry technique with different cooling rates to obtain the experimental C_V data over a reduced temperature range $3\times 10^{-6} \leqslant |T/T_c-1| < 10^{-2}$. The microgravity SF_6 C_V data were recently reanalyzed using a renormalization group theory prediction [18]. The critical temperature $T_c=318.6804$ K was obtained from this reanalysis which is within the stated uncertainty of 0.5 mK from the global minimum $T_c=318.6801$ K or the local minimum $T_c=318.6800$ K of Haupt and Straub [17]. Because the renormalization group theory prediction is valid in the crossover region, all the available experimental data were used in determining the critical temperature. Thus, any systematic errors near T_c were reduced in the reanalysis. Using this newly determined critical temperature, the experimental data systematically curved below (above) the theoretical prediction up to 3% for T higher (lower) than T_c for $|T/T_c-1|<1\times 10^{-5}$. In view of the long density relaxation time obtained in this study, we associate these systematic deviations from the theoretical prediction to density relaxation times that were too long (the diffusive relaxation time for SF_6 in the 19.2-mm-diam cell is estimated to be 227 h at $T/T_c-1=1\times 10^{-5}$) for the experimental ramping rates used by Haupt and Straub (the slowest was -0.06 K/h).

IV. CONCLUSION

Instead of tackling the complicated problem of simulating the temperature and density equilibration in the flight cell as shown in Fig. 1 (a task most probably out of reach of today's capabilities in terms of near-critical fluids simulation), we have studied the temperature and density equilibration in a composite system of just one near-critical fluid layer in contact with a copper plate of the same geometry. A general analytical solution has been found for this composite problem. This solution shows that the equilibration can be characterized by three distinct regimes. (i) The piston-effect-dominated regime within which over 99% temperature equilibration is finished in seconds for $T>T_c$ [the characteristic time for this regime is given by Eqs. (A3)–(A5)]. (ii) A transverse diffusion regime for the 3D model within which transverse inhomogeneity in the fluid relaxes diffusively [the characteristic time for this regime is given by Eq. (1)]. (iii) Finally, a radial diffusion regime for the 3D model within which radial inhomogeneity in the composite fluid-solid system relaxes diffusively and becomes less than 0.05% [the characteristic time for this regime is given by Eq. (3)]. Note that the solution obtained is valid only in the linear regime when the amplitude of the heating is small compared to the initial reduced temperature. In the case of a large temperature change between an initial reduced temperature and a final one, the global relaxation time will be shorter than the longer of the two relaxation times as predicted for each of these reduced temperatures. Based on this observation, we can always predict a safe (if not precise) value of the relaxation time, even when the heating is strong and the linear model is inapplicable. Besides, any buoyancy-driven or *g*-jitter-driven convection in a microgravity environment will only speed up the equilibration and shorten the timetable of the flight experiment. Therefore our predictions represent a worst-case estimate for a typical timetable of a flight experiment.

Owing to the geometry—i.e., $d \ll R$—our analysis shows that the heat transfer in helium during the first two regimes is little influenced by a change in the copper thickness (although the relaxation dynamics are intrinsically very differ-

ent from a pure 1D situation). In the third regime, however, the remaining radial inhomogeneity relaxes by conduction through the copper. Our 3D solution shows that the radial equilibration time can be shortened by half if the copper plate thickness is doubled, agreeing with the intuitive expression for $\tau_{\text{radial}}^{\text{comp}}$ given in Eq. (3). Hence, a change in the copper thickness can have an effect on the typical relaxation times, but only in the third (and longest) regime. On the other hand, increasing the copper thickness will be of no help in shortening the measurement time if the amplitude of the fluid inhomogeneity is sufficiently small at the end of the second regime for a given experiment.

Our 3D solution also identifies the characteristic length scales for each regime, enabling us to estimate temperature and density relaxation times in the coexisting phases by using the average specific heat at constant pressure in Eq. (3). We consider this determination of the characteristic length scale to be an important achievement of our study, since developing a complete model of the coexisting phase problem would be significantly more complicated. In the case of the proposed flight cell design, the analysis presented here suggests that specific heat experiments near the liquid-gas critical point could be successfully performed during the anticipated time period for a microgravity flight.

ACKNOWLEDGMENTS

We are grateful to Dr. M. Moldover for bringing up the issue of the composite radial relaxation. We are also grateful to Dr. I. Hahn for helpful discussions regarding the relaxation issue.

APPENDIX A: SIMPLE MODEL TO JUSTIFY NEARLY ISOTHERMAL COPPER

The large thermal conductivity of the copper leads to a rapid radial relaxation time for a composite system, but its finite value results in a radial temperature gradient within the copper plate. Using qualitative arguments, we will first show that, even in a thin copper plate, the radial temperature gradient in the copper should be much smaller than the gradients present in helium fluid, so the copper plate can still be considered essentially isothermal.(*r*)

When the circumference boundary temperature of the composite system is raised by ΔT, we assume that the heat required to raise the helium temperature goes into the fluid layer uniformly via the copper plate through surface contact. The amount of heat required for the portion of the helium within an arbitrary radius $r<R$ is $\Delta Q(r)=\pi r^2 \times d_{\text{He}}(\rho C_V)_{\text{He}}\Delta T$. Here, the heat stored in the copper plate can be ignored since its heat capacity is much smaller than that of the fluid. We assume the heat $\Delta Q(r)$ is delivered through the copper at radius r over the time period of one transverse diffusive relaxation time $\Delta t=\tau_{\text{transverse}}$. Thus, the heat conduction equation in the copper plate can be approximated as

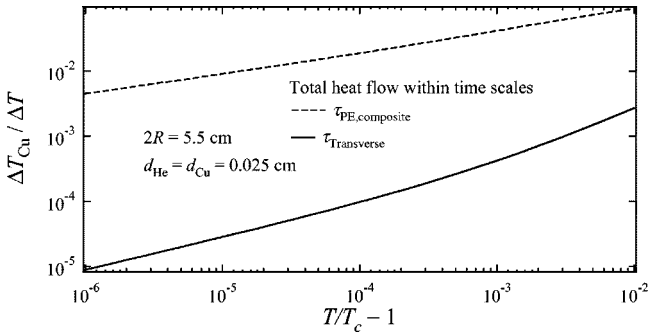

FIG. 13. The radial temperature difference within the copper plate, scaled by the step boundary temperature change, versus reduced temperature for two heat-flow time scales.

$$2\pi r d_{\text{Cu}}\lambda_{\text{Cu}} \left.\frac{dT_{\text{Cu}}}{dr}\right|_r = \frac{\Delta Q(r)}{\Delta t} = \frac{\pi r^2 d_{\text{He}}(\rho C_V)_{\text{He}}\Delta T}{\tau_{\text{transverse}}}. \tag{A1}$$

By integrating Eq. (A1), the resultant radial temperature difference within the copper from the circumference to the center can then be calculated as

$$\frac{\Delta T_{\text{Cu}}}{\Delta T} = \frac{T_{\text{Cu}}(R) - T_{\text{Cu}}(0)}{\Delta T} = \left(\frac{C_V}{C_P}\right)_{\text{He}} \frac{\lambda_{\text{He}}}{\lambda_{\text{Cu}}} \frac{R^2}{4 d_{\text{He}} d_{\text{Cu}}}. \tag{A2}$$

In reality, the heat flow into the helium at early times is much faster because of the piston effect [1]. A more stringent test of the copper temperature gradient is obtained by using the modified piston time in place of $\tau_{\text{transverse}}$ as the time scale for the heat flow. The modified piston time $\tau_{\text{PE,composite}}$ of the composite system is given by [10]

$$\tau_{\text{PE,composite}} = t_1 \frac{1+\sigma}{\sigma}, \tag{A3}$$

with

$$t_1 = \frac{(\rho C_P)_{\text{He}}}{\lambda_{\text{He}}} \left(\frac{C_V d}{C_P}\right)_{\text{He}}^2, \tag{A4}$$

where the inverse impedance ratio is

$$\sigma = \frac{\lambda_{\text{Cu}}}{\lambda_{\text{He}}} \left(\frac{D_{\text{He}}}{D_{\text{Cu}}}\right)^{1/2}, \tag{A5}$$

with D_{He} and D_{Cu} being the thermal diffusivity of fluid helium and copper, respectively. This improved time scale gives

$$\frac{\Delta T_{\text{Cu}}}{\Delta T} = \frac{T_{\text{Cu}}(R) - T_{\text{Cu}}(0)}{\Delta T} = \frac{\lambda_{\text{He}}}{\lambda_{\text{Cu}}} \frac{R^2}{4 d_{\text{He}} d_{\text{Cu}}} \frac{\sigma}{1+\sigma}. \tag{A6}$$

Figure 13 shows the radial temperature difference within the copper plate, scaled by the step boundary temperature change ΔT, versus reduced temperature for the two special cases given above. These cases correspond to heat being transferred into the fluid helium within (1) a modified piston time $\tau_{\text{PE,composite}}$ (dashed curve) and (2) a thermal diffusion time $\tau_{\text{transverse}}$ (solid curve). In these calculations, we used $\lambda_{\text{Cu}}=2$ W/cm K and $(\rho C_P)_{\text{Cu}}=5.6\times 10^{-4}$ J/cm^3 K at

$T=3.3$ K. As the critical temperature T_c is approached, the total heat required for a ΔT boundary temperature change increases only slightly $[\propto(\rho C_V)_{\mathrm{He}}]$. On the other hand, the time scale (either $\tau_{\mathrm{tranverse}}$ or the modified piston time $\tau_{\mathrm{PE,composite}}$ increases much faster than $(\rho C_V)_{\mathrm{He}}$. Therefore the radial heat flux within the copper plate decreases as T_c is approached. This leads to a decreasing radial temperature difference within the copper plate as the transition is approached. The copper plates are closer to being isothermal near the transition, with $\Delta T_{\mathrm{Cu}}/\Delta T$ being less than 1% for $T/T_c-1<10^{-4}$ using the modified piston time. Because it predicts nearly isothermal copper, this simple model suggests that the true relaxation time is close to the faster $(\tau_{\mathrm{transverse}})$ limit shown in Fig. 2.

APPENDIX B: DETAILED TEMPERATURE CALCULATIONS IN LAPLACE SPACE

Equation (13) is an expression in temporal space for the temperature in copper plate. Equation (19) is an expression in Laplace space for the temperature in helium fluid. Both equations contain undetermined coefficients. In this appendix, we derived analytical expressions for these coefficients in Laplace space by matching the heat flux and temperature at the interface between helium and copper.

1. Matching between helium and copper

The matching condition at the interface between helium and copper requires that both the temperature and the heat flux be continuous at $\tilde{z}=\bar{z}=0$. For flux continuity, one has

$$\frac{\lambda_{\mathrm{He}}}{d_{\mathrm{He}}/2}\frac{\partial\tilde{T}}{\partial\tilde{z}}(\tilde{z}=0)=\frac{\lambda_{\mathrm{Cu}}}{d_{\mathrm{Cu}}/2}\frac{\partial\bar{T}}{\partial\bar{z}}(\bar{z}=0) \tag{B1}$$

or

$$\frac{\partial\tilde{T}}{\partial\tilde{z}}(\tilde{z}=0)=\Lambda\frac{\partial\bar{T}}{\partial\bar{z}}(\bar{z}=0), \tag{B2}$$

with $\Lambda=(\lambda_{\mathrm{Cu}}/\lambda_{\mathrm{He}})(d_{\mathrm{He}}/d_{\mathrm{Cu}})$, which is typically larger than 1. However, no asymptotic simplification is possible based on this observation. Indeed, the flux continuity requires that a solution for a general value of Λ be found (otherwise, only degenerate solutions can be obtained, where the copper remains isothermal to first order). Substituting Eq. (13) for $\bar{T}$ and Eq. (19) for $\tilde{T}$ into Eq. (B2), one has

$$b(p,r)\sqrt{p}\sinh(\sqrt{p})=\Lambda\sum_{1}^{+\infty}A_n(p)C_nH\sinh(C_nH)J_0(C_nr), \tag{B3}$$

where $A_n(p)$ denotes the Laplace transform of $a_n(t)$. From the temperature continuity $\tilde{T}(\tilde{z}=0)=\bar{T}(\bar{z}=0)$, one has

$$\frac{\gamma-1}{\gamma}\langle\tilde{T}\rangle+b(p,r)\cosh(\sqrt{p})=\frac{1}{p}-\sum_{1}^{+\infty}A_n(p)\cosh(C_nH)J_0(C_nr). \tag{B4}$$

One now needs to define $1/p$ in terms of the Bessel functions $J_0(C_nr)$. This is accomplished using the orthogonality property

$$\int_0^1 rJ_0(C_nr)J_0(C_mr)dr=0 \quad \text{if } n\neq m, \tag{B5}$$

$$\int_0^1 rJ_0(C_nr)J_0(C_nr)dr=\frac{1}{2}J_1^2(C_n). \tag{B6}$$

When unity is expanded as a sum of the Bessel functions,

$$1=\sum_{1}^{+\infty}D_nJ_0(C_nr), \tag{B7}$$

the scalar product defined in Eqs. (B5) and (B6) and leads to

$$D_n=\frac{2}{J_1^2(C_n)}\int_0^1 rJ_0(C_nr)dr \tag{B8}$$

or

$$D_n=\frac{2}{C_nJ_1(C_n)}. \tag{B9}$$

Hence one has

$$\frac{1}{p}=\frac{1}{p}\sum_{1}^{+\infty}\frac{2}{C_nJ_1(C_n)}J_0(C_nr). \tag{B10}$$

Equation (B10) is valid everywhere except at $r=0$ and $r=1$ where the Bessel series are singular. Combining Eqs. (B3), (B4), and (B10), one obtains

$$A_n=\left(\frac{1}{p}-\frac{\gamma-1}{\gamma}\langle\tilde{T}\rangle\right)\times\frac{2}{C_nJ_1(C_n)}\frac{\sqrt{p}}{\Lambda C_nH\sinh(C_nH)\coth(\sqrt{p})+\sqrt{p}\cosh(C_nH)}. \tag{B11}$$

The expressions for dimensionless temperatures in the copper and fluid helium become

$$\bar{T}(r,\bar{z},p)=\frac{1}{p}-\sum_{1}^{+\infty}A_n(p)\cosh[C_nH(\bar{z}-1)]J_0(C_nr), \tag{B12}$$

$$\tilde{T}(r,\tilde{z},p) = \frac{\gamma-1}{\gamma}\langle\tilde{T}\rangle + \frac{\cosh[\sqrt{p}(\tilde{z}+1)]}{\sqrt{p}\sinh(\sqrt{p})}\Lambda H \times\sum_{1}^{+\infty} A_n(p)C_n\sinh(C_nH)J_0(C_nr) = \frac{\gamma-1}{\gamma}\langle\tilde{T}\rangle + \left(\frac{1}{p} - \frac{\gamma-1}{\gamma}\langle\tilde{T}\rangle\right) \times\cosh[\sqrt{p}(\tilde{z}+1)]\sum_{1}^{+\infty} B_n(p)J_0(C_nr), \quad \text{(B13)}$$

with

$$B_n = \frac{2}{J_1(C_n)}\frac{\Lambda H}{\Lambda C_nH\cosh(\sqrt{p}) + \sqrt{p}\sinh(\sqrt{p})\mathrm{ctanh}(C_nH)}. \quad \text{(B14)}$$

Using Eq. (B13), the spatial average of the temperature distribution in helium, $\langle\tilde{T}\rangle$, can be derived. First, the spatial average of a function in cylindrical coordinates is defined as

$$\langle f(r,\tilde{z})\rangle = -\int_0^{-1}\left[\frac{1}{\pi}\int_0^1 2\pi r f(r,\tilde{z})dr\right]d\tilde{z}. \quad \text{(B15)}$$

Substituting the spatial dependence of Eq. (B13) into Eq. (B15), one has

$$\langle\cosh[\sqrt{p}(\tilde{z}+1)]J_0(C_nr)\rangle = -2\int_0^{-1}\cosh[\sqrt{p}(\tilde{z}+1)]d\tilde{z}\int_0^1 rJ_0(C_nr)dr = \frac{\sinh(\sqrt{p})}{\sqrt{p}}\frac{2J_1(C_n)}{C_n}. \quad \text{(B16)}$$

Hence we have

$$\langle\tilde{T}\rangle = \frac{\gamma-1}{\gamma}\langle\tilde{T}\rangle + \left(\frac{1}{p} - \frac{\gamma-1}{\gamma}\langle\tilde{T}\rangle\right)\sum_{1}^{+\infty} B_n\frac{\sinh(\sqrt{p})}{\sqrt{p}}\frac{2J_1(C_n)}{C_n}. \quad \text{(B17)}$$

This leads to

$$\langle\tilde{T}\rangle(p) = \frac{\gamma}{p}\frac{\sum_{1}^{+\infty} E_n}{1+(\gamma-1)\sum_{1}^{+\infty} E_n}, \quad \text{(B18)}$$

with

$$E_n = B_n\frac{\sinh(\sqrt{p})}{\sqrt{p}}\frac{2J_1(C_n)}{C_n} = \frac{4}{C_n\sqrt{p}}\frac{\Lambda H}{\Lambda C_nH\mathrm{ctanh}(\sqrt{p}) + \sqrt{p}\mathrm{ctanh}(C_nH)}. \quad \text{(B19)}$$

The Laplace coefficients for the copper temperature are given by Eq. (B11). The expression for the helium temperature in the Laplace space is given by Eq. (B13). Both equations contain the average temperature in the helium, which is given in Eq. (B18). The problem is now solved in Laplace space. One needs only to invert the Laplace transforms to obtain the temperature profiles and average temperature at any given time.

APPENDIX C: TEST CASES OF THE GENERAL SOLUTION

The solution obtained for the temperature and density relaxation in a 3D system is a complex series of Laplace transforms. As such, it is difficult to accurately assess its validity. In order to justify the exactness of the result, we have relied on two asymptotic limits: the behavior of the series when the copper becomes a perfect heat conductor and the behavior of the series when the heat transfer in the fluid becomes purely diffusive.

If the copper plates are perfect heat conductors, the temperature in the interior of the plates will relax instantly and will remain isothermal throughout the fluid evolution. The temperature relaxation in the fluid will then be governed by a pure 1D piston effect along the transverse direction (variable z). This situation is obtained for the limit $\Lambda H^* \to \infty$.

If this limit is applied to Eqs. (B14) and (B19), one finds

$$B_n \to \frac{2}{C_nJ_1(C_n)}\frac{1}{e^{2\sqrt{p}}+1}, \quad \text{(C1)}$$

$$E_n \to \frac{1}{\sqrt{p}}\frac{4}{C_n^2}\frac{e^{\sqrt{p}}-e^{-\sqrt{p}}}{e^{\sqrt{p}}+e^{-\sqrt{p}}}. \quad \text{(C2)}$$

Based on the property

$$\sum_{1}^{+\infty}\frac{4}{C_n^2} = 1,$$

the temperature solution in Eq. (B13) becomes

$$\tilde{T} \to \frac{1}{p}\frac{e^{\sqrt{p}(\tilde{z}+1)} + e^{-\sqrt{p}(\tilde{z}+1)} + \frac{\gamma-1}{\sqrt{p}}(e^{\sqrt{p}} - e^{-\sqrt{p}})}{e^{\sqrt{p}} + e^{-\sqrt{p}} + \frac{\gamma-1}{\sqrt{p}}(e^{\sqrt{p}} - e^{-\sqrt{p}})}. \quad \text{(C3)}$$

The above expression is the Laplace transform of the general piston effect 1D solution, when both the piston effect and diffusion are taken into account [as obtained by a direct resolution of Eq. (16) in 1D geometry] [19]. The pure 1D piston effect is thus obtained as a special case of our 3D solution.

The second test for the general solution is to apply the limit $\Lambda \to 0$. In this case, the specific heats at constant pressure and constant volume are equal, and the piston effect disappears. The obtained solution should thus describe a purely diffusive transport in a 3D cylindrically symmetric composite cell. If $\gamma=1$, Eq. (B13) becomes

$$\tilde{T}(r,\tilde{z},p) = \frac{1}{p}[e^{-\sqrt{p}(\tilde{z}+1)} + e^{\sqrt{p}(\tilde{z}+1)}]\sum_{1}^{+\infty} B_n(p)J_0(C_nr). \quad \text{(C4)}$$

A direct 3D diffusive solution (similar to the one presented here but not detailed in this paper) leads to the exact same

result [20]. Hence, our solution becomes equivalent to a purely diffusive one in the case of an incompressible fluid.

The two particular limit cases described above give us confidence in the reliability of the general set of solutions.

APPENDIX D: NUMERICAL INVERSION OF THE LAPLACE SERIES

The general solution of the problem is obtained under the form of an infinite series of Laplace transforms involving Bessel functions of order zero and one. Such solutions must rely on numerical inversion to be expressed in the space of physical variables (r,z,t). In order to do so, the series are first truncated at a certain number of terms, summed up as complex functions of the complex variable p, and then the inverse Laplace transform of the obtained complex function is computed. The Laplace inversion is based on the Durbin formula combined with the epsilon algorithm [21]. The chosen relative precision in our calculations was 10^{-6}. Note that the inversion always fails at $r=0$ and $r=1$: it is well known indeed that Bessel series are singular in these two values of the radial variable. Very close to these values though, convergence is recovered, so that the prediction of the fluid's behavior is possible essentially everywhere in the cell despite these singularities.

Let us examine the convergence of the solution when the number of truncated terms in the series is increased. A test at a reduced temperature of 10^{-6} was conducted. This reduced temperature, which is the smallest we used in our calculation, leads to the slowest convergence of the series due to the thinnest boundary layers. At a given dimensionless time t and for $r=0.2$ and $\tilde{z}=-1$ (middle plane of the fluid layer, close to the center of the cell), the numerical inversion was conducted for a sum of 10–100 terms in steps of 10. Figure 14 shows the difference in convergence between each successive calculation. For a given N, the value plotted is the difference between the temperature calculated with N terms and the temperature calculated with $N-10$ terms at the same point and at the same time. This value thus represents the correction brought by adding 10 more terms to the series after rank N. As can be seen on the figure, this correction becomes smaller and smaller as the rank at which the series is truncated (i.e., N) increases, until it finally levels off around 10^{-6} when N becomes larger than 80. This saturation of the correction at 10^{-6} is due to the error in the numerical inversion of the Laplace transform, chosen to be 10^{-6} as mentioned above. Hence, regardless of the number of terms included in the estimate of the series, an error of this order will always be observed. Similar figures have been drawn for other reduced temperatures and dimensionless times, with equivalent results.

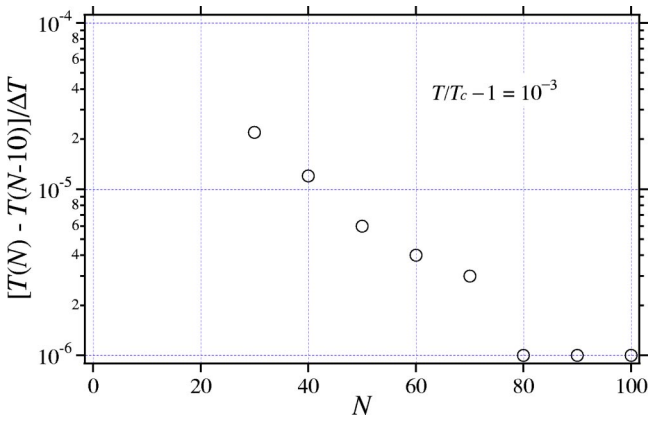

FIG. 14. Convergence of numerical Laplace inversion versus the number of terms in the series for a reduced temperature of 10^{-3}.

In all the figures presented in this article, the series were truncated after $N=100$ terms and the Laplace inversion was conducted with a relative precision of 10^{-6}.

[1] A. Onuki and R. Ferrell, Physica A **164**, 245 (1990).
[2] A. Onuki, H. Hao, and R. A. Ferrell, Phys. Rev. A **41**, 2256 (1990).
[3] H. Boukari, J. N. Shaumeyer, M. E. Briggs, and R. W. Gammon, Phys. Rev. A **41**, 2260 (1990).
[4] B. Zappoli, D. Bailly, Y. Garrabos, B. Le Neindre, P. Guenoun, and D. Beysens, Phys. Rev. A **41**, 2264 (1990).
[5] H. Boukari, R. Pego, and R. Gammon, Phys. Rev. E **52**, 1614 (1995).
[6] F. Zhong and H. Meyer, Phys. Rev. E **51**, 3223 (1995).
[7] J. Straub and L. Eicher, Phys. Rev. Lett. **75**, 1554 (1995).
[8] B. Zappoli and P. Carlès, Eur. J. Mech. B/Fluids **14**, 41 (1995).
[9] R. F. Berg, Phys. Rev. E **48**, 1799 (1993).
[10] R. A. Ferrell and H. Hao, Physica A **197**, 23 (1993).
[11] M. Barmatz, Inseob Hahn, Fang Zhong, M. A. Anisimov, and V. A. Agayan, J. Low Temp. Phys. **121**, 633 (2000).
[12] M. Barmatz (unpublished).
[13] P. Carlès, Phys. Fluids **10**, 2164 (1998).
[14] P. Carlès and K. Dadzie (unpublished).
[15] R. A. Wilkinson *et al.*, Phys. Rev. E **57**, 436 (1998).
[16] F. Zhong and H. Meyer, Phys. Rev. E **53**, 5935 (1996).
[17] A. Haupt and J. Straub, Phys. Rev. E **59**, 1795 (1999).
[18] M. Barmatz, F. Zhong, and A. Shih, Int. J. Thermophys. **34**, 1 (2004).
[19] P. Carlès (unpublished).
[20] P. Carlès (unpublished).
[21] R. Piessens and R. Huysman, ACM Trans. Math. Softw. **10**, 348 (1984).